analytical chemistry

Article

pubs.acs.org/ac

# Analytical Cumulative Exam Dec 2019

S. Cologna

Instructions: The following article has been recently published in the journal *Analytical Chemistry*. Your assignment is to read the article, write the abstract and give the article a title. You will be scored upon your concise ability to write the abstract to reflect the article as well as the appropriateness of the title. Total points 10 points. Passing is 7 points.

Grading:
Title - 2pts
Intro to technique - 2pts
Problem being addressed & major findings - 5 pts
Concluding statement - 1pt

Surface enhanced Raman spectroscopy (SERS) provides molecular fingerprint information down to the single-molecule level with exceptionally high specificity. Furthermore, SERS inherits the high spectral resolution, short response time, low sample pretreatment requirements, and measurement conveniency under ambient/aqueous conditions of Raman spectroscopy. Thus, these merits provide many opportunities for its application in various disciplines, such as analytical chemistry,[1,2] physical chemistry,[3,4] materials,[5,6] energy systems,[7] and biomedical science.[8,9] In recent years, SERS has become an attractive ultrasensitive quantitative analysis technique that commonly includes solid substrate-based or nanoparticle (NP) sol-based analysis techniques[10] being widely used to detect proteins,[11,12] nucleic acids,[13,14] and small molecules and in biomedicine.[15−17] However, quantitative SERS analysis is plagued by poor measurement reproducibility caused by the uneven distribution of, enhancement generating, plasmonic hot spots on SERS active substrates. Additionally, Raman signals are easily affected by environmental test conditions.

Thus, various attempts have been made to improve the accuracy and reliability of quantitative SERS analysis techniques. Ratiometric SERS assays and internal standards (ISs) have been employed to normalize volatility in SERS signals caused by variations in the physical properties of SERS substrates. Ratiometric SERS quantitative analysis requires the target analyte to react with a SERS probe molecule immobilized on the surface of enhancement active substrates. From this, accurate quantitative results of the analyte can be acquired by deformation of spectral bands, provided there are no competing adsorption processes, but it is uncommon and impractical to have an appropriate SERS probe for every analyte of interest; therefore, ratiometric SERS is limited in the scope of its applications.[18,19] Introducing an IS can solve the above problem, and many research groups have reported meaningful results.[20−25] For instance, the Yang group[26] utilized 4-mercaptopyridine as an IS to correct signal fluctuations and improve substrate stability for the quantitative detection of various drugs. However, such IS molecules are immobilized on the surface of enhancement active substrates by coordinate or electrostatic interactions and thus suffer from competitive adsorption and microenvironmental effects.

**Received:** August 14, 2019
**Accepted:** November 4, 2019
**Published:** November 4, 2019

Recently, core-molecular-shell (CMS) NPs with integrated IS molecular shells have attracted interest as ideal IS materials for quantitative SERS assays,[27−31] exhibiting desirable properties such as 1) enhancement of both substrate and IS signals, 2) no competition between the IS and analytes at adsorption sites, and 3) no IS shell influences on the spatial distribution or the Raman signals of analytes in the external environment. However, CMS nanostructures are complicated as IS molecules and need to be assembled on the surface of the metal NP cores; moreover, controlling and modifying IS molecules are not a facile process. The Tan group[32] actualized an accurate quantitative SERS analysis technique using stable graphene-isolated-Au-nanocrystals, where the graphene shell was the IS. However, the characteristic D and G bands from graphene introduced background signals which could overlap with analyte signals; similarly, the synthesis process was complicated and time-consuming. Table S1 summarized a comparison of these materials used for quantitation.

Based on the above, developing efficient and novel materials coating methods remains an urgent requirement for developing quantitative SERS techniques to better analyze important systems. Prussian blue (PB) is a blue dye, containing Fe(II) and Fe(III) ions and the cyanide ($-CN^-$) group, with excellent magnetic, electrical, and optical properties, that has been widely used in energy storage,[33] catalysis,[34] and biomedicine.[35] PB is a highly sensitive and background free resonant Raman tag that displays a sharp and strong single peak in the traditionally Raman-silent region of the spectrum. PB-based surface enhanced Raman resonant spectroscopic (SERRS) tags have also been used as highly sensitive immunoassays and in cancer cell imaging.[36] However, there have been no reports employing PB as an IS to improve the accuracy of quantitative SERS analysis.

Herein, we successfully applied ultrathin layer(s) of PB, which acted as a coating/shell, on Au NPs to form Au@PB NPs. These novel core−shell NPs showed a strong characteristic PB Raman vibrational band at 2155 $cm^{-1}$. Unlike many other IS probes, this PB spectral band is in the Raman silent region, thus significantly reducing the chance of signal overlap and interference with analyte signals and is suitable for use as an IS for SERS quantitative analysis of complex systems. Additionally, because of their stable and robust signals, Au@PB NPs are not subject to photobleaching or photoquenching effects. Based on this core−shell NP structure, we quantitatively detected crystal violet (CV) and dopamine (DA) analyte concentrations in lake water and blood serum, respectively, evidencing a facile, convenient, label-free, cost-effective, stable, and rapid SERS platform for quantitative analysis of complex systems with "real-world" applications.

## EXPERIMENTAL SECTION

**Materials and Apparatus.** Chloroauric acid hydrate ($HAuCl_4{\cdot}4H_2O$), CV, sodium citrate, ascorbic acid, iron(III) chloride hexahydrate ($FeCl_3{\cdot}6H_2O$), potassium hexacyanoferrate(III) ($K_3[Fe(CN)_6]$), potassium hexacyanoferrate(II) trihydrate ($K_4[Fe(CN)_6]{\cdot}3H_2O$), nitric acid, ethanol, hydrogen peroxide, *N*,*N*′-dimethylformamide (DMF), hydrochloric acid, *n*-hexane, and sulfuric acid were purchased from Sinopharm Chemical Reagent Co., Ltd. (Shanghai, China). Tetrabutylammonium nitrate ($TBA^+NO_3^-$), DA, 2,6-pyridinedicarboxylic acid, and rhodamine 6G (R6G) were obtained from Sigma-Aldrich (St. Louis, MO, U.S.A.). All experimental glassware was washed with aqua regia before use. Ultrapure Milli-Q water (18.2 MΩ·cm) was used to make up all experimental solutions. Blood serum samples were acquired with permission from Hangzhou Medical College Hospital.

**Apparatus and Characterization.** A Hitachi S-4800 scanning electron microscope (SEM) was applied to observe the morphology of the Au@PB NPs, and a JEM-2100 transmission electron microscope (TEM) was used to check the PB shell. High resolution scanning transmission electron microscopy (HR-TEM) and scanning transmission electron microscopy-energy dispersive X-ray spectrometry (STEM-EDS) elemental mapping analysis on a Tecnai F30 (FEI, U.S.A.) were applied to further observe Au@PB NPs. Raman spectra were recorded by an Xplora Raman spectrometer (Xplora, France), with a 633 nm laser (power density, 100%), an exposure time of 1, 10, and 30 s, a grating of 1200/mm, and a 50× objective lens (NA 0.55). UV−visible absorption spectroscopy was performed on a UV-2700 UV−vis spectrophotometer (Shimadzu, Japan). Solution injection rates were controlled by a laboratory microinjection pump (LSP01-1A, China).

**Preparation of Au NPs.** Fifty nanometer spherical Au NPs were prepared by a two-step growth method similar to our previously described method.[37] First, 16 nm spherical Au NP seeds were synthesized by the classical reduction scheme after minor modification.[38,39] A total of 100 mL of $HAuCl_4$ aqueous solution (wt 0.01%) was poured into a 200 mL round-bottom flask and then heated to boiling under stirring. Subsequently, 3.0 mL of sodium citrate solution (wt 1.0%) was added to the above boiling solution. The second step was to prepare 50 nm Au NPs; 24 mL of 16 nm of Au seed solution and 160 mL of Milli-Q water were added to a 200 mL round-bottom flask, and then 4.8 mL of ascorbic acid (wt 1.0%) and 1.6 mL of sodium citrate solution (wt 1.0%) were added to the above solution and continuously stirred in an ice bath. After that, 8.8 mL of $HAuCl_4$ solution (wt 0.825%) was added dropwise to the solution at a rate of 0.4 mL/min by the step motor at room temperature and then heated at 70 °C for 20 min.

**Synthesis of Au@PB NPs.** Au@PB NPs with various shell thicknesses were prepared by double-precursor synthesis with slight modifications.[36] An aqueous solution of $K_3[Fe(CN)_6]$ (0.5 mmol/L) was added to the 50 nm Au NPs solution and stirred for 5 min; after that, the surfaces of Au NPs were etched by $CN^-$. Subsequently, suitable volumes of $K_4[Fe(CN)_6]$ and $FeCl_3{\cdot}6H_2O$ of the same concentration (0.1 mmol/L) were simultaneously added dropwise to the above solution at a rate of 0.1 mL/min by the step motor at room temperature. The Au@PB NPs were washed three times with Milli-Q water and centrifuged (6500 rpm, 10 min). Then, the Au@PB NPs were redispersed in ultrapure water and concentrated 10 times.

**Structural Stability of Au@PB NPs.** For stability experiments, the effects of pH and temperature were investigated. A volume of 20 μL of Au@PB NPs was mixed with 180 μL of disodium hydrogen phosphate-citrate buffer solution at different pH values (2.2, 3.2, 4.2, 5.2, 6.2, 7.5, and 8.0). After 120 min, the above solution was transferred to a quartz cuvette for Raman analysis, and the morphology of NP was observed by TEM. Twenty microliter volumes of Au@PB NPs solutions were placed in an oven at different temperatures (50 °C, 100 °C, 130 °C) for 1 h, respectively, and then Milli-Q water was added to make up the volumes to 200 μL before being used for Raman analysis. Copper grids with appropriate amounts of Au@PB NPs applied were also put in the above


DOI: 10.1021/acs.analchem.9b03703
Anal. Chem. 2019, 91, 15025−15031

oven at the same temperatures and heated for 1 h, for morphological characterization by TEM.

**SERS Detection Performance Optimization.** The experimental conditions, including the amount of Au@PB NPs and the incubation time of Au@PB NPs with analytes, were examined and optimized using CV as the target analyte. Twenty microliters of the same concentration of CV was mixed with different amounts of Au@PB NPs (5.0 $\mu$L, 10 $\mu$L, 20 $\mu$L, and 30 $\mu$L); after 30 min, the above solution was transferred to a quartz cuvette for Raman analysis. For time measurements, 20 $\mu$L of the Au@PB NP solution was mixed with 160 $\mu$L of water and transferred to a quartz cell, then 20 $\mu$L of CV was added to the above solution, and Raman was started immediately and then recorded every 5 min. Except for an exposure time of 1 s, other conditions of Raman analysis were the same as above.

**SERS Activity of the Au@PB NPs.** Raman spectra of three analytes (CV, DA, and R6G) were collected, respectively, in both the presence and absence of Au@PB NPs. Raman spectra were collected of low (2.0 nmol/L) and high (0.5 mmol/L) concentration CV solutions with and without Au@PB NPs, respectively. Furthermore, Raman spectra of low concentration (500 nmol/L) and high concentration (1.0 mmol/L and 1.0 mol/L) DA solutions with and without Au@PB NPs were also collected. Finally, Raman spectra of low (1.0 nmol/L) and high concentration (0.2 mmol/L) R6G with and without Au@PB NPs were also measured. For DA solutions, except for an exposure time of 30 s, all other conditions for the Raman tests were the same as CV.

**SERS Measurement in Dispersions.** For SERS measurements in ultrapure Milli-Q water, 20 $\mu$L of various concentrations of analyte was mixed with 20 $\mu$L of Au@PB NPs in 160 $\mu$L of water for 15 min. Subsequently, the obtained solution was transferred to a quartz cell. The cell was then placed on the Xplora Raman spectrometer for Raman spectral acquisitions. Every measurement was the average value of 2 scans, and experiments for each sample at each concentration were repeated 3 times. For all the measurements, the laser intensity of the sample was 15 mW with a 633 nm laser. The exposure time for each scan was 10 s. For SERS measurement of blood serum and lake water, 20 $\mu$L of lake water or blood serum containing various concentrations of analytes was mixed with 20 $\mu$L of Au@PB NPs and 160 $\mu$L of Milli-Q water for 15 min; the subsequent experimental procedure was the same as outlined above.

## RESULTS AND DISCUSSION

**SERS Quantification Scheme, Morphology, and Spectral Properties of Au@PB NPs.** Figure 1A shows schematically the synthesis procedure of Au@PB NPs substrates with analytes for quantitative SERS analysis. First, 50 nm diameter Au NP cores were prepared by a two-step method, described above. Subsequently, Au NP surfaces were etched with $K_3[Fe(CN)_6]$ for 5 min enabling PB shell assembly on Au NP surfaces after 10 min to form the Au@PB NPs. Analytes were then adsorbed onto the surfaces of Au@PB NPs via electrostatic forces, enabling their direct SERS detection in a cuvette similar to simple UV−vis spectroscopic measurements.

Au@PB core−shell NPs with various PB shell thicknesses were prepared by adjusting the concentration of aqueous $K_4[Fe(CN)_6]$ and $FeCl_3{\cdot}6H_2O$, as well as addition rates. TEM images in Figure 1B show the PB shell thickness could be

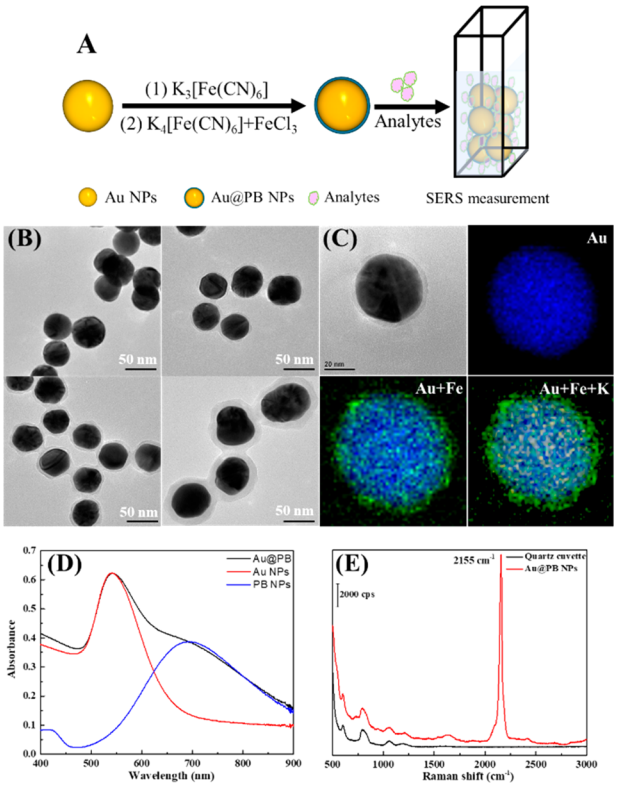


**Figure 1.** (A) Schematic illustrating the synthesis procedure of Au@PB NPs-based substrates for SERS quantification analysis of analytes in solution. (B) TEM images of Au@PB core−shell NPs with various (~2−12 nm) shell thicknesses. (C) HRTEM images of Au@PB NPs, with an ~4 nm PB shell, and EDS elemental mapping of Au core (blue) independently as well as with Fe (green) and K (yellow) in merged images. (D) UV−vis absorption spectrum of Au NPs (red), PB NPs (blue), and Au@PB NPs (black). (E) Raman spectra of Au@PB NPs with ~2−3 nm PB shell and quartz cuvette.

adjusted from 2 to 12 nm. Considering that the shell thickness impacts on the Raman signal intensity of the analyte, a thin PB shell (2−3 nm) gave optimal enhancement of analyte Raman signals. As shown in Figure S1, TEM images clearly show ultrathin PB was deposited on Au NPs, where PB acts as a protective shell and offers an IS for quantitative SERS analysis. The Au@PB NPs were further examined by HRTEM and STEM-EDS elemental mapping analysis. As shown in Figure 1C, the ~4 nm PB shell is clearly visible from HRTEM, which also indicates the successful synthesis of the core−shell structure of Au@PB NPs. From STEM-EDS elemental mapping images, it can be seen that Fe and K elements from PB were evenly distributed on the Au surface, indicating that the Au core is evenly covered with a PB shell. The morphologies of Au@PB NPs were also observed by SEM in Figure S2, and it can be seen that the Au@PB NPs could be prepared with high yields and excellent uniformity.

As shown in Figure 1D, for the Au@PB NPs, there are two absorption peaks located at 540 and 700 nm for Au NPs and PB NPs, respectively. For Au@PB NPs, these bands were combined and further demonstrate successful synthesis of the core−shell NPs. Moreover, the plasmonic resonance absorbance peak for PB located from 600 to 800 nm is in resonance with the Raman laser excitation wavelengths of 638 and 785 nm. This resonance effect greatly improves the Raman signal of PB. According to zeta potential measurements, the Au@PB

NPs were negatively charged (Figure S3, $\zeta$ = −15.3 mV), which promotes electrostatic adsorption of positively charged analytes species. As shown in Figure 1E, an intense and sharp single Raman peak at 2155 $cm^{-1}$ for the Au@PB NPs is observed, located in the Raman silent region. This unique characteristic band of PB makes it an ideal IS for quantitative SERS analysis studies. In addition, Au@PB NPs can interact and join with one another (Figures 1B and S1) to form junctions. These junctions between NPs generate the necessary plasmonic hot spots in the bulk solution dispersions without the need for additional agglomerating agents. These results suggest that Au@PB NPs have the extremely advantageous property of being useable as enhancing substrates in different dispersions for quantitative SERS measurements with "real-world" applications.

**Structural Stability of Au@PB NPs.** Making stable and homogeneous SERS substrates that do not interfere with analyte signals remains a challenge in SERS analysis. Herein, the structural stability and integrity of Au@PB NPs were investigated under acidic, basic, and high-temperature conditions. As shown in Figure 2A, the PB Raman band at

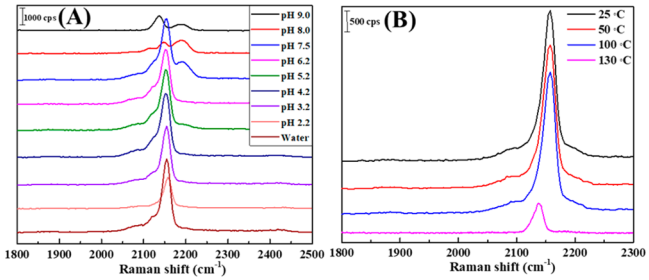


**Figure 2.** Structural stability of Au@PB NPs. (A) The influence of pH on the Raman signal of the PB shell, where the pH is 2.2, 3.2, 4.2, 5.2, 6.2, 7.5, 8.0, and 9.0. (B) The effect of temperature on the Raman signal of the PB shell.

2155 $cm^{-1}$ was observed from pH values of 2.2 to 9.0, and the Au@PB NPs exhibited excellent signal stability from pH 3.2 to 7.5. However, the PB Raman band at 2155 $cm^{-1}$ was not observed at a pH greater than 8.0. These results were also examined by TEM in Figure S4; the PB shell is a little soluble at pH 2.2 and largely dissolved at a pH greater than 8.0. Also, the influence of temperature on the Raman signal of the PB shell was investigated. As can be seen from Figure 2B, the Raman signal of the PB shell at 2155 $cm^{-1}$ remained stable from 25 to 100 °C and then disappeared, and a new Raman band at 2137 $cm^{-1}$ appeared at 130 °C. It was confirmed by TEM in Figure S5, that the PB shell was damaged at high temperatures. Furthermore, compared with ultrapure water systems, the stability of Au@PB NPs in complex "real-world" systems, e.g., in lake water and serums (discussed in detail later), was also investigated. PB Raman signals in these complex systems remained nearly unchanged, indicating excellent stability under various conditions (Figure S9 and Figure S10). Above all, these results show that the Au@PB NPs remain stable and intact within a general set of reasonable test conditions, thus offering the possibility of detecting analytes in various complex and biological systems.

**Determining SERS Activity of the Au@PB NPs.** To evaluate the SERS activity of Au@PB NPs, the Raman signals of three analytes (CV, DA, R6G) were collected in the presence or absence of Au@PB NPs, respectively. As can be seen from Figure 3A, multiple characteristic CV Raman bands are visible at low concentrations with Au@PB NPs present,

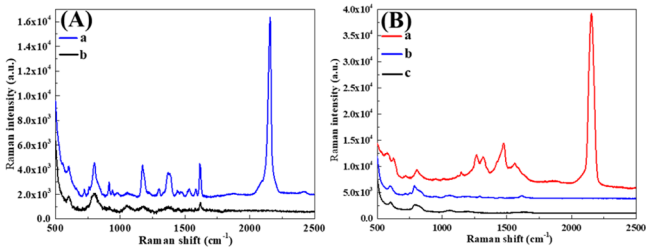


**Figure 3.** (A) SERS spectra of (a) CV (2.0 × $10^{-6}$ mmol/L) with Au@PB NPs and (b) normal CV (0.5 mmol/L) without Au@PB NPs. (B) SERS spectra of (a) DA (5.0 × $10^{-4}$ mmol/L) with Au@PB NPs, (b) normal DA (1000 mmol/L), and (c) DA (1.0 mmol/L) without Au@PB NPs.

and these signals are much greater than those without Au@PB NPs in solution. Furthermore, no DA Raman signals are observed without Au@PB NPs, even when higher concentrations up to 1.0 mol/L were used (Figure 3B). However, in the presence of Au@PB NPs, even at low concentrations of 500 nmol/L, multiple characteristic DA Raman bands are clearly visible. These obvious differences in concentration sensitivity indicate that the Au@PB NPs in solution generate abundant SERS-active hot spots, offering strong SERS signals owing to good analyte adsorption on NPs via electrostatic interactions. Finally, R6G was selected as a model Raman analyte to evaluate the enhancement factor (EF) (Figure S6). The EF at the R6G peak at 1510 $cm^{-1}$ was calculated to be 0.8044 × $10^6$ for Au@PB NPs based on the equation outlined in Figure S6.[40−42]

**SERS Signal Detection Optimization.** To achieve the best analytical performance for SERS detection, CV was selected as a target analyte. The experimental conditions including the amount of Au@PB NPs and the incubation time of Au@PB NPs with CV were examined and optimized. As shown in Figure S7, the SERS intensity of the IS Raman band ($I_{2155\ cm^{-1}}$) of PB increased gradually with an increase in the concentration of Au@PB NPs; however, the ratio between the Raman intensities of the 1617 $cm^{-1}$ CV band and the 2155 $cm^{-1}$ IS band ($I_{1617\ cm^{-1}}/_{2155\ cm^{-1}}$) reached a maximum when the volume of Au@PB NPs was 20 $\mu$L (Figure 4A). Therefore, 20 $\mu$L was the optimum volume of Au@PB NPs used in these systems. Figure S8 shows the SERS signal of CV in the

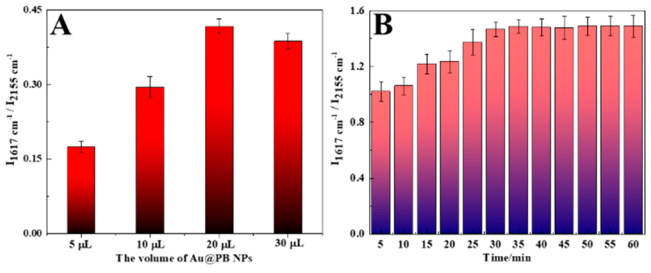


**Figure 4.** (A) The relationship between the Raman intensity ratio $I_{1617\ cm^{-1}}/_{2155\ cm^{-1}}$ vs the volume of Au@PB NPs. Error bars represent the statistical relative standard deviation (RSD) of triplicate SERS experiments. (B) The relationship between the $I_{1617\ cm^{-1}}/_{2155\ cm^{-1}}$ vs the incubation time. Error bars represent the statistical relative standard deviation (RSD) of triplicate SERS experiments.



DOI: 10.1021/acs.analchem.9b03703
Anal. Chem. 2019, 91, 15025−15031

presence of Au@PB NPs as a function of the incubation time, with the SERS signal of CV increasing with increasing incubation time. As can be seen in Figure 4B, after 35 min the $I_{1617\ cm^{-1}}/_{2155\ cm^{-1}}$ ratio reached a maximum value and remained unchanged thereafter. Therefore, 35 min was chosen as the optimal incubation time.

**Quantitative SERS Measurements of CV Analyte Concentrations.** CV is a cheap triphenylmethane dye that has been widely used in textile and printing industries owing to its aesthetically beautiful violet color. In addition, CV has also been widely used by the pharmaceutical industry and in veterinary medicine as it is effective at preventing fungal and parasite infections in aquacultures. However, the above applications have resulted in pollution due to the discharge of CV into effluent waters which increases vestigial traces of CV in aquaculture products. In the European Union, the presence of CV in food is prohibited as high doses can be carcinogenic.[43,44] Many approaches for determining CV concentrations in water have been proposed.[45−47] However, most of these are inefficient and expensive, as well as being complicated and time-consuming to operate. Thus, the development of highly sensitive, facile, rapid, and reliable methods for detecting residual CV in effluent waters is an important research objective.

Herein, core−shell Au@PB NPs are proposed as enhancing substrates for detecting CV Raman signals adjacent to the NPs. The PB shell in the Au@PB NPs can absorb CV nearby, moreover, the PB shell displays the SERS signal at 2155 $cm^{-1}$, which is ideal for use as an IS to normalize fluctuations in CV signals due to concentration. Thus, herein, successful quantitative SERS detection of CV with Au@PB NPs is illustrated. Using the same volume of Au@PB NPs in all experiments, the Raman spectra of solutions containing varying concentrations of CV from 2.0 to 100 nmol/L were collected and are shown in Figure 5A. The major peaks at 1617 and 1586 $cm^{-1}$ are assigned to the ring C−C stretch, and those at 724 and 799 $cm^{-1}$ are assigned to the out-of-plane vibrations of ring C−H. Additionally, the peaks around 916 and 1171 $cm^{-1}$ are assigned to the ring skeletal vibrations of the radical orientation and in-plane vibrations of ring C−H, respectively.[48] The SERS intensity of the 1617 $cm^{-1}$ band gradually increased with an increase in CV concentration, while the intensity of the 2155 $cm^{-1}$ PB band only fluctuated slightly between different concentrations of CV. The merits of using PB as the IS are evidenced in Figure 5B and Figure 5C, where the plot of $I_{1617\ cm^{-1}}/_{2155\ cm^{-1}}$ vs Log [CV concentration] represents the relationship between the ratio of Raman peak intensity for CV (1617 $cm^{-1}$) and PB (2155 $cm^{-1}$) vs the Log of CV concentration (Log [CV concentration]). While the $I_{1617\ cm^{-1}}$ vs Log [CV concentration] plot shows the relationship between the CV peak intensity at 1617 $cm^{-1}$ vs Log [CV concentration]. Compared with the $I_{1617\ cm^{-1}}$ vs Log [CV concentration] plot, the $I_{1617\ cm^{-1}}/_{2155\ cm^{-1}}$ vs Log [CV concentration] plot displayed a relatively better linear fit and higher precision; furthermore, signals for concentrations as low as 2.0 nmol/L of CV could be readily collected.

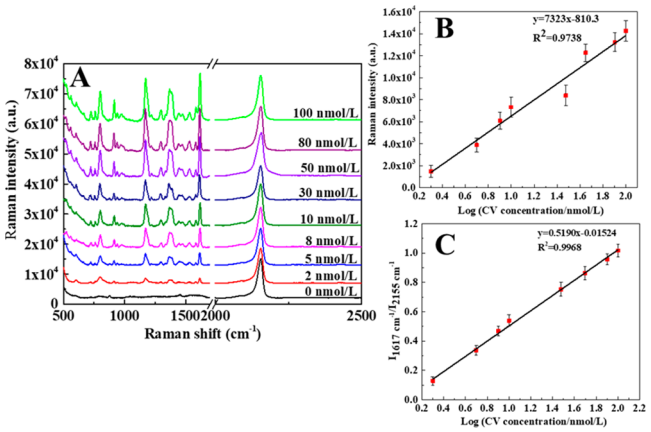


**Figure 5.** (A) SERS spectra of various concentration of CV (0, 2.0, 5.0, 8.0, 10, 30, 50, 80, and 100 nmol/L). (B) Calibration plot based on Raman intensity at 1617 $cm^{-1}$ vs Log [CV]. (C) Calibration plot based on the Raman intensity of $I_{1617\ cm^{-1}}/_{2155\ cm^{-1}}$ vs Log [CV]. Error bars signify the RSD of three independent experiments.

Having established that Au@PB NPs are capable of structural stability in complex systems and can accurately detect different CV concentrations, we further applied Au@PB NPs to measure CV concentrations in a lake within our university campus. A series of CV in the lake water samples were analyzed; all lake water samples were spiked with CV at three different concentration levels and then analyzed by the proposed method. The results listed in Figure S9 and Table S2 show satisfactory measurements with an acceptable accuracy range between 94.6%−108.8%, and RSDs lower than 7.0%. The above results indicate that Au@PB NPs as IS-SERS substrates can offer a useful and promising means for monitoring CV in complex systems.

**Quantitative SERS Measurements of DA Concentrations.** For showing the versatility and general applicability of Au@PB NPs-based SERS assays; detection of other analytes by Au@PB NPs was also investigated. DA is a well-known catecholamine neurotransmitter present in mammalian brain tissue and body fluids, which plays a significant role in regulating central nervous, vascular, and hormonal systems.[49] Abnormal levels of the DA concentrations *in vivo* are associated with various pathologic conditions such as Parkinson's, Alzheimer's, and Huntington's diseases. Clinically, determining DA concentrations in biological fluids is significant for the prevention and treatment of DA-related diseases as well as the monitoring of brain functions.[50] Thus, a highly sensitive and accurate technique for determining DA concentrations in complex biological fluids is extremely important and helpful for understanding biological processes. Thus, developing reliable and facile methods for quantitatively detecting DA concentrations in various biological matrices is an important ongoing challenge.[51,52]

Similarly, the same SERS methodology for quantitatively detecting CV concentrations described in detail above, i.e., Au@PB NPs, was used to quantitatively measure DA concentrations. Raman spectra were obtained by mixing Au@PB NPs with various concentrations of DA dissolved in water. It can be seen from Figure 6A, in which the fingerprint SERS peaks at 807, 1148, 1267, and 1475 $cm^{-1}$ were assigned to DA,[53,54] that the intensity of the 1475 $cm^{-1}$ peak (C−H bond in aliphatic chain) gradually increases with an increase in DA solution concentrations. Figure 6B shows a plot of the quantitative calibration curve for the intensity of the 1475 $cm^{-1}$ SERS peak ($I_{1475\ cm^{-1}}$) versus the concentration of DA [DA], and a plot of the ratio of the DA and PB SERS intensities ($I_{1475\ cm^{-1}}/_{2155\ cm^{-1}}$) vs [DA] is shown in Figure 6C. An extremely good linear fit in the concentration range between 500 and 8000 nmol/L with a linear correlation

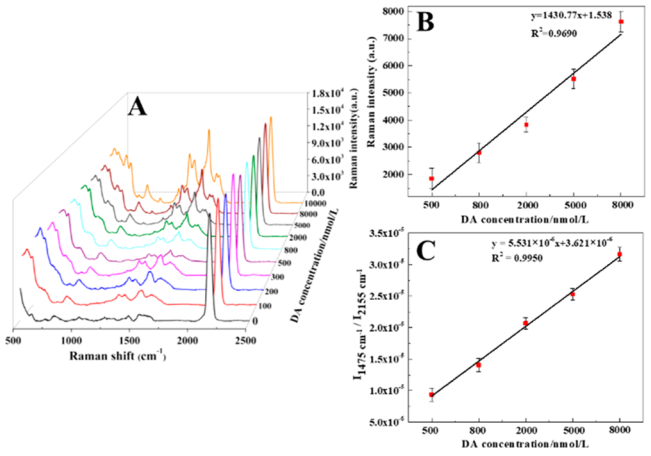


**Figure 6.** (A) SERS spectra of this system at various concentrations of DA (0, 100, 200, 300, 500, 800, 2000, 5000, 8000, and 10000 nmol/L). (B) Calibration plot based on Raman intensity at 1479 $cm^{-1}$ vs [DA]. (C) Calibration plot based on the Raman intensity of $I_{1475\ cm^{-1}}/_{2155\ cm^{-1}}$ vs [DA]. Error bars are derived from the RSD of three independent experiments.

coefficient of 0.9950 was obtained, with concentrations as low as 100 nmol/L being detectable (Figure 6A). The good detection performance may be due to the affinity of Fe(III) of Au@PB NPs and DA, and Au@PB NPs serve as a sensitive SERS probe for detection of DA molecules.[55−57]

We then investigated the potential of Au@PB NPs as SERS substrates for quantitative analysis of practical systems, i.e., DA concentrations in blood serum. All blood serum samples were spiked with DA at three different concentration levels and then analyzed with the proposed method. The results listed in Figure S10 and Table S3 show satisfactory recoveries in the range of 90.9%−107.5% and an acceptable accuracy with RSDs below 7.0%. The above results indicate that Au@PB NPs as IS-SERS substrates could offer a useful and promising means of monitoring DA levels in complex biological fluids.

## CONCLUSIONS

In summary, we synthesized ultrathin core−shell Au@PB NPs with good SERS enhancements and an IS for facile and reliable quantitative SERS analysis of multiple analytes in different fluids. The Au@PB NPs were composed of a Au core and a PB shell, which integrated the unique Raman enhancement, generated by the Au core, as a clear way to distinguish the Raman signal of PB which was used as an intrinsic IS. This IS-SERS method showed potentially promising practical applications for the direct quantitative determination of CV concentrations in lake water and DA concentrations in blood serum. In addition, Au@PB NPs were shown to have relatively good pH and temperature stability and could be used for the immediate detection of analytes in complex fluids without the need for pretreatment. The PB shell demonstrated a single, strong, and unique Raman vibration band at 2155 $cm^{-1}$, in the tyipically Raman silent spectral region, which was used as an excellent IS with low liklihood for overlap with the analyte fingerprint spectral bands, reducing inaccuracies when studying complex systems. Furthermore, the PB shell also showed excellent stability and excellent quantitative accuracy for SERS analysis. Above all, Au@PB NPs were shown to be excellent SERS enhancement substrates for the precise quantification of analyte concentrations, which holds great potential to be applied in important complex and practical systems.

## ASSOCIATED CONTENT

### Supporting Information

The Supporting Information is available free of charge on the ACS Publications website at DOI: 10.1021/acs.analchem.9b03703.

Additional experimental results, morphologies and zeta potential of Au@PB NPs, SERS activity and structural stability of Au@PB NPs, calibration plot of CV in lake and DA in serum, and recovery experiments of CV in lake samples and DA in serum (PDF)

## AUTHOR INFORMATION

### Corresponding Author

*Phone: +86-592-2186192. E-mail: li@xmu.edu.cn.

**ORCID**

### Notes

The authors declare no competing financial interest.

## ACKNOWLEDGMENTS

This work was supported by NSFC (21775127, 21703187, and 21427813), the Fundamental Research Funds for the Central Universities (20720190044 and 20720170102), the State Key Laboratory of Fine Chemicals (KF1702), and the Open Fund of the State Key Laboratory of Luminescent Materials and Devices (South China University of Technology).

## REFERENCES

(1) Nie, S.; Emory, S. R. *Science* **1997**, *275*, 1102−1106.
(2) Shafer-Peltier, K. E.; Haynes, C. L.; Glucksberg, M. R.; Van Duyne, R. P. *J. Am. Chem. Soc.* **2003**, *125*, 588−593.
(3) Choi, H. K.; Park, W. H.; Park, C. G.; Shin, H. H.; Lee, K. S.; Kim, Z. H. *J. Am. Chem. Soc.* **2016**, *138*, 4673−4684.
(4) Xi, W. J.; Haes, A. *J. Am. Chem. Soc.* **2019**, *141*, 4034−4042.
(5) Dick, S.; Konrad, M. P.; Lee, W. W. Y.; McCabe, H.; McCracken, J. N.; Rahman, T. M. D.; Stewart, A.; Xu, Y. K.; Bell, S. E. J. *Adv. Mater.* **2016**, *28*, 5705−5711.
(6) Li, C. Y.; Le, J. B.; Wang, Y. H.; Chen, S.; Yang, Z. L.; Li, J. F.; Cheng, J.; Tian, Z. Q. *Nat. Mater.* **2019**, *18*, 697−701.
(7) Dong, J. C.; Zhang, X. G.; Martos, V. B.; Jin, X.; Yang, J.; Chen, S.; Yang, Z. L.; Wu, D. Y.; Feliu, J. M.; Williams, C. T.; Tian, Z. Q.; Li, J. F. *Nat. Energy* **2019**, *4*, 60−67.
(8) Pallaoro, A.; Mirsafavi, R. Y.; Culp, W. T. N.; Braun, G. B.; Meinhart, C. D.; Moskovits, M. *Nanomedicine* **2018**, *14*, 1279−1287.
(9) Zong, C.; Xu, M. X.; Xu, L. J.; Wei, T.; Ma, X.; Zheng, X. S.; Hu, R.; Ren, B. *Chem. Rev.* **2018**, *118*, 4946−4980.
(10) Bell, S. E. J.; Sirimuthu, N. M. S. *Chem. Soc. Rev.* **2008**, *37*, 1012−1024.
(11) Tran, V.; Walkenfort, B.; König, M.; Salehi, M.; Schlücker, S. *Angew. Chem., Int. Ed.* **2019**, *58*, 442−446.
(12) Deb, S. K.; Davis, B.; Knudsen, G. M.; Gudihal, R.; Ben-Amotz, D.; Davisson, V. J. *J. Am. Chem. Soc.* **2008**, *130*, 9624−9625.
(13) Wang, X.; Choi, N.; Cheng, Z.; Ko, J.; Chen, L. X.; Choo, J. *Anal. Chem.* **2017**, *89*, 1163−11697.
(14) Sun, Y.; Li, T. *Anal. Chem.* **2018**, *90*, 11614−11621.
(15) Li, X.; Lee, H. K.; Phang, I. Y.; Lee, C. K.; Ling, X. Y. *Anal. Chem.* **2014**, *86*, 10437−10444.
(16) Haddad, A.; Comanescu, M. A.; Green, O.; Kubic, T. A.; Lombardi, J. R. *Anal. Chem.* **2018**, *90*, 12678−12685.

(17) Fornasaro, S.; Bonifacio, A.; Marangon, E.; Buzzo, M.; Toffoli, G.; Rindzevicius, T.; Schmidt, M. S.; Sergo, V. *Anal. Chem.* **2018**, *90*, 12670−12677.
(18) He, S.; Kyaw, Y. M. E.; Tan, E. K. M.; Bekale, L.; Kang, M. W. C.; Kim, S. S. Y.; Tan, I.; Lam, K. P.; Kah, J. C. Y. *Anal. Chem.* **2018**, *90*, 6071−6080.
(19) Wang, W.; Zhang, L. M.; Li, L.; Tian, Y. *Anal. Chem.* **2016**, *88*, 9518−9523.
(20) Tian, L.; Su, M. K.; Yu, F. F.; Xu, Y.; Li, X. Y.; Li, L.; Liu, H. L.; Tan, W. H. *Nat. Commun.* **2018**, *9*, 3642.
(21) Yu, Q.; Wang, Y. Q.; Mei, R. C.; Yin, Y. C.; You, J. M.; Chen, L. X. *Anal. Chem.* **2019**, *91*, 5270−5277.
(22) Song, Z. L.; Dai, X.; Li, M. R.; Song, Z.; Chen, Z.; Luo, X. L. *Chem. Commun.* **2018**, *54*, 8618−8621.
(23) Zhang, D. M.; Xie, Y.; Deb, S. K.; Davison, V. J.; Ben-Amotz, D. *Anal. Chem.* **2005**, *77*, 3563−3569.
(24) Stosch, R.; Henrion, A.; Schiel, D.; Guttler, B. *Anal. Chem.* **2005**, *77*, 7386−7392.
(25) Yin, P. G.; Jiang, L.; Lang, X. F.; Guo, L.; Yang, S. H. *Biosens. Bioelectron.* **2011**, *26*, 4828−4831.
(26) Yan, X. N.; Zhou, B. B.; Tang, X. H.; Li, X. Y.; Weng, S. Z.; Yang, L. B.; Liu, J. H. *Anal. Chem.* **2017**, *89*, 4875−4881.
(27) Shen, W.; Lin, X.; Jiang, C. Y.; Li, C. Y.; Lin, H. X.; Huang, J. T.; Wang, S.; Liu, G. K.; Yan, X. M.; Zhong, Q. L.; Ren, B. *Angew. Chem., Int. Ed.* **2015**, *54*, 7308−7312.
(28) Gandra, N.; Singamaneni, S. *Adv. Mater.* **2013**, *25*, 1022−1027.
(29) Song, J. B.; Duan, B.; Wang, C. X.; Zhou, J. J.; Pu, L.; Fang, Z.; Wang, P.; Lim, T. T.; Duan, H. W. *J. Am. Chem. Soc.* **2014**, *136*, 6838−6841.
(30) Lim, D. K.; Jeon, K. S.; Hwang, J. H.; Kim, H.; Kwon, S.; Suh, Y. D.; Nam, J. M. *Nat. Nanotechnol.* **2011**, *6*, 452−460.
(31) Feng, Y. H.; Wang, Y.; Wang, H.; Chen, T.; Tay, Y. Y.; Yao, L.; Yan, Q. Y.; Li, S. Z.; Chen, H. Y. *Small* **2012**, *8*, 246−251.
(32) Zhang, Y.; Zou, Y. X.; Liu, Y.; Xu, Y. T.; Wang, X. W.; Li, Y. J.; Liang, H.; Chen, L.; Chen, Z.; Tan, W. H. *Anal. Chem.* **2016**, *88*, 10611−10616.
(33) Wu, M. S.; He, L. J.; Xu, J. J.; Chen, H. Y. *Anal. Chem.* **2014**, *86*, 4559−4565.
(34) Indra, A.; Paik, U.; Song, T. *Angew. Chem., Int. Ed.* **2018**, *57*, 1241−1245.
(35) Qin, Z. G.; Li, Y.; Gu, N. *Adv. Healthcare Mater.* **2018**, *7*, 1800347.
(36) Yin, Y. M.; Li, Q.; Ma, S. S.; Liu, H. Q.; Dong, B.; Yang, J.; Liu, D. B. *Anal. Chem.* **2017**, *89*, 1551−1557.
(37) Li, J. F.; Huang, Y. F.; Ding, Y.; Yang, Z. L.; Li, S. B.; Zhou, X. S.; Fan, F. R.; Zhang, W.; Zhou, Z. Y.; Wu, D. Y.; Ren, B.; Wang, Z. L.; Tian, Z. Q. *Nature* **2010**, *464*, 392−395.
(38) Frens, G. *Nature, Phys. Sci.* **1973**, *241*, 20−22.
(39) Guerrero, A. R.; Aroca, R. F. *Angew. Chem., Int. Ed.* **2011**, *50*, 665−668.
(40) Xu, Y. K.; Konrad, M. P.; Lee, W. W. Y.; Ye, Z. W.; Bell, S. E. J. *Nano Lett.* **2016**, *16* (8), 5255−5260.
(41) Le Ru, E. C.; Blackie, E.; Meyer, M.; Etchegoin, P. G. *J. Phys. Chem. C* **2007**, *111*, 13794−13803.
(42) Ujihara, M.; Dang, N. M.; Imae, T. *Sensors* **2017**, *17*, 2563.
(43) Mani, S.; Bharagava, R. N. *Rev. Environ. Contam. Toxicol.* **2016**, *237*, 71−104.
(44) Tighe, A.; Johnson, V. L.; Taylor, S. S. *J. Cell Sci.* **2004**, *117*, 6339−6353.
(45) Roy, S.; Mohd-Naim, N. F.; Safavieh, M.; Ahmed, M. U. *ACS Sens.* **2017**, *2*, 1713−1720.
(46) Li, J.; Zhu, Z.; Zhu, B. Q.; Ma, Y. L.; Lin, B. Q.; Liu, R. D.; Song, Y. L.; Lin, H.; Tu, S.; Yang, C. Y. *Anal. Chem.* **2016**, *88*, 7828−7836.
(47) Davis, D.; Portelius, E.; Zhu, Y.; Feigerle, C.; Cook, K. D. *Anal. Chem.* **2005**, *77*, 8151−8154.
(48) He, L.; Kim, N. J.; Li, H.; Hu, Z.; Lin, M. *J. Agric. Food Chem.* **2008**, *56*, 9843−9847.
(49) Zhang, A.; Neumeyer, J. L.; Baldessarini, R. J. *Chem. Rev.* **2007**, *107*, 274−302.
(50) Ji, X.; Palui, G.; Avellini, T.; Na, H. B.; Yi, C.; Knappenberger, K. L.; Mattoussi, H. *J. Am. Chem. Soc.* **2012**, *134*, 6006−6017.
(51) Jiang, Z. W.; Gao, P. F.; Yang, L.; Huang, C. Z.; Li, Y. F. *Anal. Chem.* **2015**, *87*, 12177−12182.
(52) Chen, J.; Li, Y.; Huang, Y.; Zhang, H.; Chen, X.; Qiu, H. *Microchim. Acta* **2019**, *186*, 58.
(53) Wang, P.; Xia, M.; Liang, O.; Sun, K.; Cipriano, A. F.; Schroeder, T.; Liu, H.; Xie, Y. H. *Anal. Chem.* **2015**, *87*, 10255−10261.
(54) Silwal, A. P.; Lu, H. P. *ACS Chem. Neurosci.* **2018**, *9*, 3117−3127.
(55) Ranc, V.; Markova, Z.; Hajduch, M.; Prucek, R.; Kvitek, L.; Kaslik, J.; Safarova, K.; Zboril, R. *Anal. Chem.* **2014**, *86*, 2939−2946.
(56) Kaya, M.; Volkan, M. *Anal. Chem.* **2012**, *84*, 7729−7735.
(57) Li, P.; Ge, M. H.; Cao, C. T.; Lin, D. Y.; Yang, L. B. *Analyst* **2019**, *144*, 4526−4533.